Mechanical Properties and Thermal Stability of Ultrathin Molybdenum Disulfide Nanowires

Chuan Chen[1], Shin-Pon Ju*[2,3], and Bo-Yuan Liao[2]

Keywords: Molecular dynamics simulation, MoS_2 nanowire

Notes

Chuan Chen[1] is with Department of Information Management, Meiho University, Pingtung 912, Taiwan(e-mail: chchen@meiho.edu.tw).

Shin-Pon Ju*[2,3] is with the Department of Mechanical and Electro-Mechanical Engineering, National Sun Yat-sen University, Kaohsiung 804, Taiwan and the Department of Medicinal and Applied Chemistry, Kaohsiung Medical University, Kaohsiung, Taiwan 807 (corresponding author's phone: +886-75252000#4231; e-mail: jushin-pon@mail.nsysu.edu.tw).

Bo-Yuan Liao[2] is with the Department of Mechanical and Electro-Mechanical Engineering, National Sun Yat-sen University, Kaohsiung 804, Taiwan (e-mail: m023020092@student.nsysu.edu.tw).

Abstract:

The most stable ultrathin molybdenum disulfide (MoS_2) nanowires of different cross-section radii were predicted by the simulated annealing basin-hopping (SABH) method with the Tersoff potential. Before the SABH procedure, the Tersoff potential parameters for MoS_2 were fitted by the force matching method (FMM) on the basis of bulk Mo, S, and MoS_2 material properties. Combined with the SABH method, a penalty function was imposed in the radial dimension of the nanowire to constrain all atoms to evolve along the designated axial direction of MoS2 nanowires. By molecular dynamics (MD) simulation of uniaxial tension, the mechanical properties including the Young's moduli, yielding stresses, and strengths of these MoS_2 nanowires were determined. In order to understand the feasibility of MoS_2 nanowire application on nano-devices, the thermal stability of these ultrathin MoS_2 nanowires was also investigated by the temperature elevation process by the MD simulation.

1 Introduction:

The general material properties of transition metal silicides are hard, inert, and refractory, and they also possess thermal stabilities [1]. Most of transition metal silicides are generally unaffected by the strong acids including aqua regia[2] . They also have good resistance to the corrosion of oxidation at high temperatures because of the formation of a tenacious oxide layer that passivates the surface from the further attack [3]. In addition, some nano-crystalline transition metal silicides have much wider applications for integrated circuit technology because of their novel properties including high strength, hardness, and electrical conductivity[4].

Among all transition metal silicides, zirconium silicide (ZrSi) has drawn a lot of attention for the last few years, because it could be used as a cladding material for the use as a neutron reflector in the next-generation nuclear systems such as gas-cooled fast reactors, which efficiently improve the reactor's performance and prevent the outer structural compounds from the irradiation damage by driving neutrons generated by nuclear reactions back to the core again[5]. Another important application of ZrSi material is used as a reinforcement material[6] in microelectronic devices because of its low electrical resisitivity (13-34 $\mu\Omega/cm^3$).For example, thin film of Zirconium silicides were investigated and showed the potentials in being the material of gate structure[7].

Except for the crystalline ZrSi structures, the amorphous ZrSi arrangement formed between the ZrSi interface was also reported in several previous studies[8-10]. These amorphous ZrSi materials have also attracted increasing interest in the field of superconductivity due to its highly disordered system. The highly disordered structures of an atomic arrangement over a microscopic scale of several angstroms is considered to be ineffective for pinning the fluxoid lines, because this spatial scale is much shorter than the Ginzburg-Landau coherence length which was estimated to be about 50-100 angstrom. Therefore, These characteristic features in amorphous superconductors provide a unique potential of superconductivity [11].

Since most of the applications of ZrSi are on the basis of its superior mechanical properties, it's important to further investigate the structural behaviors and atomic arrangement. Molecular dynamics (MD) simulations is a powerful tool to overcome the limitations of traditional empirical approaches and enable detailed observations of material behaviors from the atomic viewpoint. So the structure was built by MD simulation in this study. Then, the structural properties are investigated by HA index and CSRO analysis. HA index is a powerful tool to determine the local structure. For example, Li et al.[12] used the HA index to analysis the structural transformation and rearrangement of atoms during the annealing process of amorphous Ni. And for understand the affinity in ZrSi alloys system, CSRO analysis is employed. CSRO analysis uses the information of coordinate numbers and the atomic composition fraction in the alloy and determines the affinity of each element pairs. For instance, Gonza´lez et al.[13] calculated the CSRO to discuss the liquid Li-Na alloy and found that as the temperature increases, the segregating tendency weakens. Thus, for understanding the structure of ZrSi in crystal and amorphous arrangements at the atomic level, the HA index and the CSRO analysis are chosen to see the local atomic structure of the ZrSi alloys.

2 Simulation model

In order to model the Zr-Si alloy system by molecular dynamics (MD) simulation, two potential functions, tight-binding[14] and Tersoff forms[15], were used to describe the interactions between different atomic pairs. The tight-binding potential is responsible for modeling the interaction between the Zr-Zr pair, and the Si-Si and Zr-Si pairs are simulated by Tersoff potential.

The tight-binding potential form is shown as Eq. (1):

$$E_i = -\left\{\sum_j \xi^2 \exp\left[-2q\left(\frac{r_{ij}}{r_0}-1\right)\right]\right\}^{1/2} + \sum_j A\exp\left[-p\left(\frac{r_{ij}}{r_0}-1\right)\right] \quad (1)$$

Where ξ is an effective hopping integral, r_{ij} is the distance between atoms *i* and *j*, and r_0 is the first-neighbor distance.

The Tersoff potential involving both two- and three-body terms is shown as Eq.(2):

$$U_{total}^{Ter} = \sum_{i=1}^{N} E_i = \frac{1}{2}\sum_{i\neq j} V(r_{ij}) \quad (2)$$

Where E_i is the potential energy of atom *i* and $V(r_{ij})$ is the energy formed between two atoms. The term $V(r_{ij})$ is defined as:

$$V(r_{ij}) = \sum_i \sum_{j>i} f_c(r_{ij})[\, f_R(r_{ij}) + b_{ij}\, f_A(r_{ij})] \quad (3)$$

$$f_A = -B_{ij}\exp(-u_{ij} r_{ij}) \quad (4)$$

$$f_R = A_{ij}\exp(-\lambda_{ij} r_{ij}) \quad (5)$$

$$b_{ij} = (1+\beta_i^{n_i}\zeta_{ij}^{n_i})^{-1/2n_i} \quad (6)$$

$$\zeta_{ij}^{n_i} = \sum_{k\neq i,j} f_c(r_{ik}) g(\theta_{ijk}) \quad (7)$$

$$g(\theta_{ijk}) = 1 + \frac{c_i^2}{d_i^2} - \frac{c_i^2}{[d_i^2 + (h_i - \cos\theta_{ijk})^2]} \quad (8)$$

$$f_c(r_{ij}) = \begin{cases} 1, r_{ij} < R_{ij} \\ \frac{1}{2} + \frac{1}{2}\cos[\pi\frac{(r_{ij}-R_{ij})}{(S_{ij}-R_{ij})}], R_{ij} < r_{ij} < S_{ij} \\ 0, S_{ij} < r_{ij} \end{cases} \quad (9)$$

The coefficient b_{ij} corresponds to a many-body interaction and the function f_C is merely a smooth cutoff function, which limits the range of the potential. The function $g(\theta ijk)$ represents the influence of the bending angle.

The force-matching method (FMM) [16] was used to determine all parameters of tight-binding and Tersoff potentials on the basis of binding energies and elastic constants of pure elements (Zr, Si) and binary (Zr_3Si_2[17], ZrSi[18], $ZrSi_2$[19]) metal systems. These parameters can be seen in Tables 1 and 2.

After the parameters are fitted, the structures of stable ZrSi amorphous structure were obtained by the simulation anneal basin-hopping (SABH) method[20] along the search direction for the energy local-minimal structure with a higher energy. A total of 10,000 atoms (5000 Zr and 5000 Si atoms) was used for both ZrSi crystal and BMG models as shown in Figs 1(a) and 1(b).

To further understand the atomic arrangement and local atomic structure, the Honeycutt Andersen and Warren-Cowley chemical short range order (CSRO) were performed.

Table I. The parameters of the tight-binding potential for Zr-Zr

Type	***A*(eV)**	***ζ*(eV)**	***p***	***q***	***r*$_0$(Å)**
Zr-Zr	0.179	2.201	9.300	2.099	3.174

Table II. The parameters of the Tersoff potential for Si-Si, Si-Zr

Type	*Si-Si*	*Zr-Si*
A(eV)	7835.380	2251.660
B(eV)	45.087	175.073
λ	3.851	2.603
μ	1.079	1.474
β	0.429	0.468E-05
n	21.161	39.960
c	27340.700	4061.980
d	119.344	3.252
h	-0.330	-0.062
R(Å)	2.783	3.216
S(Å)	2.986	3.562

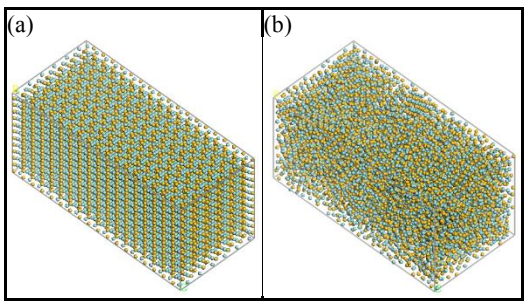

Fig. 1 The MD simulation models for (a) crystal; (b) amorphous ZrSi alloys

3 Results and Discussion

For the amorphous ZrSi structure, the x-ray diffraction (XRD) and radial distribution function (RDF) profiles are shown in Figs. 2(a) and 2(b). One can see that no specific crystalline peak appears in the 2θ range between 10° – 90° for XRD profile, and the second RDF peak of Fig. 2(b) is splitted. These characteristics indicate the ZrSi configuration constructed by SABH is amorphous.

Figure 3 shows the RDF profiles of different pairs, Zr-Zr, Si-Si, and Zr-Si, for ZrSi crystal and BMG structures. The first RDF peaks of Zr-Zr, Si-Si, Zr-Si pairs are located at 3.43, 2.49, 2.75 Å for the crystal, and situated at 3.09, 2.95, 2.73 Å for the BMG. It is clear that the Zr-Si bond lengths in crystal and

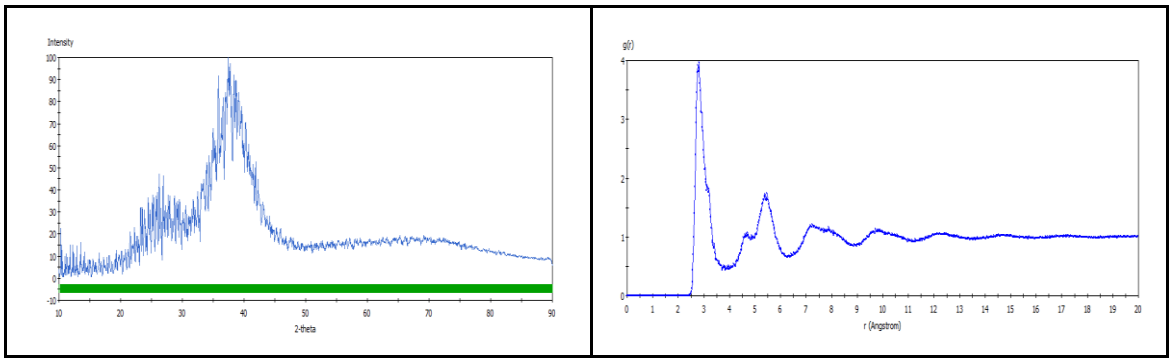

Fig. 2 (a) XRD and (b) RDF profiles for ZrSi BMG

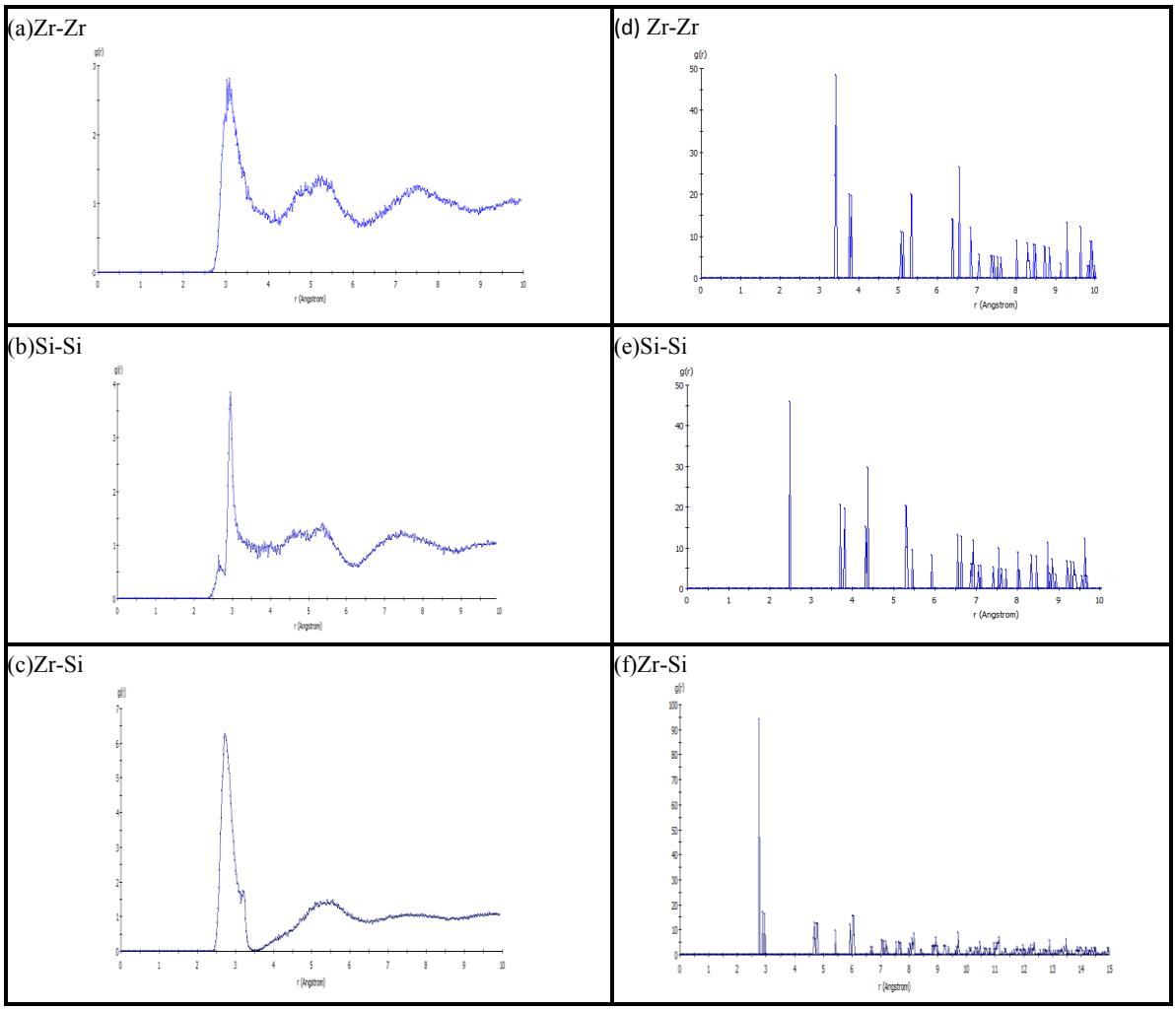

Fig. 3 The partial RDF profiles of Zr-Zr, Si-Si, and Zr-Si pairs for ZrSi BMG (a~c) and crystal (d~f).

BMG are very close. The Zr-Zr length of BMG is longer than that of crystal, whereas the Si-Si length of BMG is shorter than that of crystal.

The Warren-Cowley chemical short-range-order (CSRO) analysis[13] for ZrSi BMG was employed to quantify the attraction and objection between element pairs. Before the CSRO analysis, the information of coordination number (CN) should be prepared. Table III lists the CNs for the ZrSi crystal and BMG on the basis of different referenced atoms. It is clear the CNs of Si-Si pair of crystal and BMG are very different and Si-Si CN of BMG is higher than that of crystal by 3.5. With the CN information, the chemical affinities of a referenced atom with its first neighbor atoms are evaluated by the CSRO parameter. The definition of this parameter is as
the following equation:

$$\alpha_{ij} = 1 - \frac{N_{ij}}{c_j N_i} \tag{10}$$

Where $\boldsymbol{\alpha}_{ij}$ is the CSRO parameter of the *i*-type referenced atom related to *j*-type atom; N_{ij} is the partial CN for the *i*-type

referenced atom related to *j*-type atom; c_j and N_i are the fraction of *j*-type atom within the alloy and the average CN of *i*-type atom, respectively. The value of c_j by N_i is an ideal partial CN for the referenced *i*-type atom related to the first neighbor *j*-type atom, and this value completely depends on the respective atomic composition fraction of ZrSi. According to this analysis, it can be seen that if the alloys are the ideal solution, the value of N_{ij} should be very close to c_jN_i and let the value of α_{ij} be 0. On the other hand, the value that larger than 0 means the *j*-type atom are less prone to gather around *i*-type atom cause the value of N_{ij} is less than the number of ideal N_{ij}. For the same reason, the negative value means the *j*-type atom are prone to gather around *i*-type atom. The CSRO parameters for ZrSi BMG are listed in Table IV and the results show that the Zr and Si are more likely to gather around each other than themselves.

Table III. The coordinate numbers of the Zr-Zr, Si-Si, Si-Zr in Crystal and BMGs

	Crystal		BMGs	
Type	N_{Zr-Zr}	N_{Zr-Si}	N_{Zr-Zr}	N_{Zr-Si}
CNs	6	7	6.094	6.566
Type	N_{Si-Si}	N_{Si-Zr}	N_{Si-Si}	N_{Si-Zr}
CNs	2	7	5.535	6.998

Table IV. The parameters of CSRO for Zr-Zr, Si-Si, Si-Zr in ZrSi BMG

	BMGs	
Type	Zr-Zr	Zr-Si
α_{ij}	0.03725	-0.03725
Type	Si-Si	Si-Zr
α_{ij}	0.1167	-0.1167

HA pair analysis is an effective technique to filter out the numbers of different local structures within the simulation system by distinguishing the them by four indexes as (i,j,k,l). The HA index distribution of crystal and amorphous ZrSi alloys is shown in Fig. 4. The total HA index shows that the crystal ZrSi alloy is mainly composed by the 1311 and 1421. The 1311 represents the rhombohedra structure and the 1421 is usually found in the F.C.C. and H.C.P. crystal structures. For ZrSi BMG, the indexes of 1551, 1541, and 1431, commonly found in liquid phase, are over 50% and the main indexes of crystal phase only occupy a small amount. The 1201 is the major component of the "other index" in Fig. 4, which implies the near-free-structure. The near-free structure is a HA pair that has only two common first neighbor atoms without bonding. Thus, this indicates that there are some loose areas in the ZrSi BMG. For further understanding the local structures formed by different atomic pairs, the partial HA index is also shown in Fig. 5. The partial HA index of crystal clearly

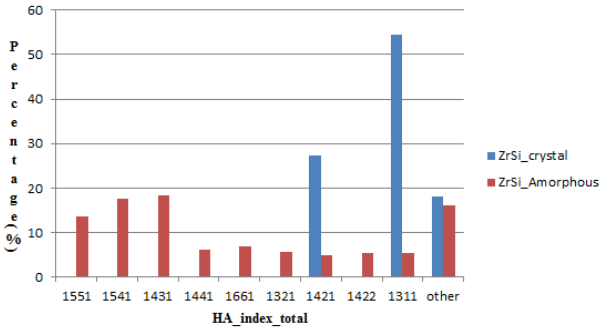

Fig. 4 HA index distributions of ZrSi BMG and crystal.

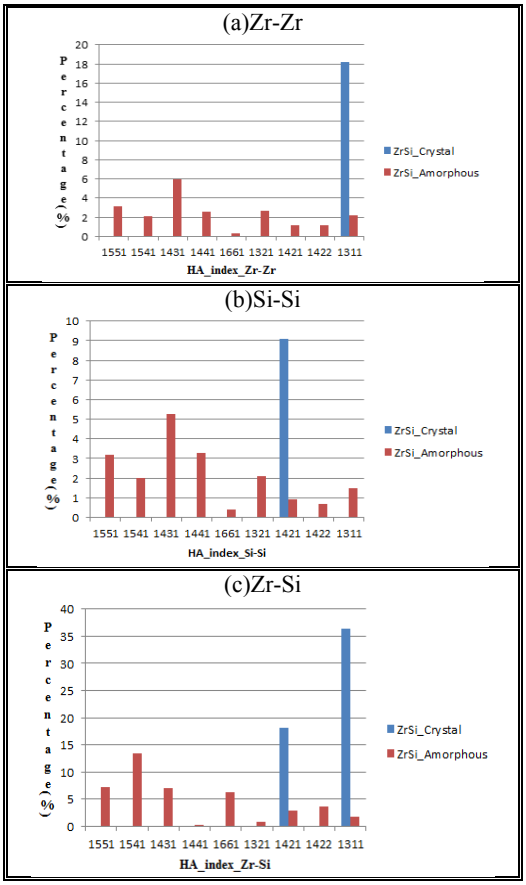

Fig. 5 HA index distributions of (a)Zr-Zr; (b)Si-Si; (c)Zr-Si pairs for ZrSi BMG and crystal.

shows that the 1311 structure is built by the cluster with Zr in the center, and 1421 is mainly composed by Si. As for the BMG, the major indexes are still 1551, 1541, 1431 for Zr-Zr, Zr-Si, and Si-Si pairs. Except for liquid states, the 1441 and 1661 which refer to BCC structure occupies quite amount of HA indexes.

4 Conclusion

The structural analysis of ZrSi crystal and BMG structures has been conducted in this study. The XRD and RDF profiles of BMG structure predicted by our SABH simulation indicate that the BMG structure is totally amorphous.

The CSRO shows that Zr and Si are more prone to gather than gathering with themselves in the alloy system. HA index shows that the 1311 and 1421 are the major indexes in the crystal ZrSi alloys. For ZrSi BMG, the 1551, 1541, 1431 referring to the liquid structure are abundant and the 1201 also occupies quite amount.

For uniaxial tension, the results show that the ZrSi BMG is more ductile than the crystal ZrSi and the ZrSi BMG deforms more uniformly than that of the crystal structure.

References

1. L. Topor and O. J. Kleppa, *Metall Trans A*, 1986, **17**, 1217-1221.
2. I. J. Cho, K. T. Park, S. K. Lee, H. H. Nersisyan, Y. S. Kim and J. H. Lee, *Chem Eng J*, 2010, **165**, 728-734.
3. J. H. Weaver, A. Franciosi and V. L. Moruzzi, *Phys Rev B*, 1984, **29**, 3293-3302.
4. I. Y. Ko, J. H. Park, J. K. Yoon, K. S. Nam and I. J. Shon, *Ceram Int*, 2010, **36**, 817-820.
5. D. Restrepo, S. M. Hick, C. Griebel, J. Alarcon, K. Giesler, Y. Chen, N. Orlovskaya and R. G. Blair, *Chem Commun*, 2013, **49**, 707-709.
6. A. Memarpour, V. Brabie and P. G. Jonsson, *Isij Int*, 2010, **50**, 1612-1621.
7. K. Pomoni and J. Salmi, *J Phys D Appl Phys*, 1991, **24**, 727-730.
8. A. Inoue, H. S. Chen, J. T. Krause and T. Masumoto, *J Non-Cryst Solids*, 1984, **68**, 63-73.
9. H. Tanaka, T. J. Konno, R. Sinclair and N. Hirashita, *Journal of applied physics*, 1995, **78**, 4982-4987.
10. J. Y. Shim, J. S. Kwak, E. J. Chi, H. K. Baik and S. M. Lee, *Thin Solid Films*, 1995, **269**, 102-107.
11. N. Toyota, A. Inoue, T. Fukase and T. Masumoto, *J Low Temp Phys*, 1984, **55**, 393-410.
12. F. Li, X. J. Liu, H. Y. Hou, G. Chen and G. L. Chen, *Journal of applied physics*, 2011, **110**.
13. D. J. Gonzalez, L. E. Gonzalez, J. M. Lopez and M. J. Stott, *Phys Rev E*, 2004, **69**.
14. F. Cleri and V. Rosato, *Phys Rev B*, 1993, **48**, 22-33.
15. J. Tersoff, *Phys Rev B*, 1989, **39**, 5566-5568.
16. F. Ercolessi and J. B. Adams, *Europhys Lett*, 1994, **26**, 583-588.
17. O. Schob, F. Benesovsky and H. Nowotny, *Monatsh Chem*, 1961, **92**, 1218-&.
18. A. Raman and K. Schubert, *Z Metallkd*, 1965, **56**, 44-52.
19. M. Setton and J. Vanderspiegel, *Journal of applied physics*, 1991, **70**, 193-197.
20. D. J. Wales and J. P. K. Doye, *J Phys Chem A*, 1997, **101**, 5111-5116.